communications physics

ARTICLE

https://doi.org/10.1038/s42005-022-01003-0 OPEN

Competition between the superconducting spin-valve effect and quasiparticle spin-decay in superconducting spin-valves

B. Stoddart-Stones [1✉], X. Montiel[1], M. G. Blamire [1] & J. W. A. Robinson [1✉]

In a ferromagnet/normal metal/ferromagnet spin-valve, spin dependent scattering causes a difference in resistance between antiparallel (AP) and parallel (P) magnetization states. The resistance difference, $\Delta R = R(AP) - R(P)$ is positive due to increased scattering of majority and minority spin-electrons in the AP-state. If the normal metal is substituted for a superconductor, the superconducting spin-valve effect occurs: in the AP-state the net magnetic exchange field acting on the superconductor is lowered and the superconductivity is reinforced meaning $R(AP)$ decreases. For current-perpendicular-to-plane spin-valves, existing experimental studies show that the normal state effect dominates ($\Delta R > 0$) over the superconducting spin valve effect ($\Delta R < 0$). Here however, we report a crossover from giant magnetoresistance ($\Delta R > 0$) to the superconducting spin-valve effect ($\Delta R < 0$) in current-perpendicular-to-plane ferromagnet/superconductor/ferromagnet spin-valves as the superconductor thickness decreases below a critical value.

[1] Department of Materials Science & Metallurgy, University of Cambridge, 27 Charles Babbage Road, Cambridge CB3 0FS, UK. ✉email: bs507@cantab.ac.uk; jjr33@cam.ac.uk

The field of spintronics[1] emerged following the discovery of spin-dependent scattering of electrons at ferromagnetic/nonmagnetic (F/N) interfaces[2] and giant magnetoresistance (GMR) in F/N/F structures[3]. In a F/N/F spin-valve, GMR is the difference in electrical resistance (ΔR) between antiparallel (AP) and parallel (P) magnetisation states of the F layers and is current-bias independent. In the AP-state, both the majority and minority spin-electrons are strongly scattered and $\Delta R = R(AP) - R(P) > 0$ with the magnitude of ΔR dependent on the spin-polarization of the F layers, interfacial spin-flip, and the spin decay length in N[4,5]. In superconducting F/S/F spin-valves[6–8] (where S is a superconductor) the superconducting critical temperature (T_c) depends on the magnetic moment orientation of the F layers due to the superconducting spin valve effect: in the P-state, the magnetic exchange fields suppress T_c(P) relative to T_c(AP), in which the magnetic exchange fields partially cancel, meaning $\Delta T_c = T_c^{AP} - T_c^{P} > 0$. This effect allows the superconducting spin-valve to act as a valve for superconducting current flow, demonstrating infinite magnetoresistance, via switching the magnetic state of a device with suitably large ΔT_c held at constant temperature. This current-bias independent behaviour is observed in current-in-plane (CIP) F/S/F spin-valves with ΔT_c reaching tens of mK for transition metal Fs[9–18] and several hundred mK for rare-earth ferromagnetic metals and insulators[19–21]. These experimental values of ΔT_c are orders of magnitude smaller than values predicted by theory[6–8], as it has proven experimentally challenging to reach the theoretically indicated optimum parameter space. Negative ΔT_c values have also been reported[14,22–30], attributed either to quasiparticle (QP) spin-accumulation[23,26,28] suppressing T_c in the AP-state[31,32], or flux penetration in S from out-of-plane domain walls in the F layers[14,24,27,30]. Other superconducting spin valves featuring a tunnel barrier have also been demonstrated[33]. Current-perpendicular-to-plane (CPP) devices have larger values of GMR than CIP devices[34–37], but are less investigated due to the extra complications of fabrication compared to CIP spin-valves, and so investigation into CPP devices with superconducting spin-valves has been limited. One reported CPP device[38] was a F/S/F spin-valve, which showed GMR behaviour ($\Delta R > 0$) due to quasiparticle transport ("QP GMR") with a reduced spin decay length relative to the normal state for superconducting Nb layer thicknesses exceeding 30 nm. We note that the superconducting spin-valve effect ($\Delta R < 0$) was not observed and that superconducting devices with thicknesses below 30 nm were not reported in that study[38].

In this article, we systematically investigate superconducting CPP F/S/F spin-valves with Py(15)/Cu(10)/Nb(d_{Nb})/Cu(10)/Py(15)/FeMn(10) layers (numbers in nm units) sandwiched between 200-nm-thick Cu electrodes (Fig. 1b). CPP devices have been used to investigate the interaction of non-equilbrium spin currents and superconductivity, by using the magnetoresistance of the CPP spin valve to quantify the spin decay through the superconductor. As expected, with decreasing Nb thickness (d_{Nb}) QP GMR increases; however, below a critical thickness of superconducting Nb ($d_{Nb} = 26$ nm) a sign change in ΔR is observed, consistent with the appearance of the superconducting spin valve effect in these CPP devices, which dominates the QP GMR behaviour at these thicknesses. We show a systematic crossover between these competing behaviours, dependent on d_{Nb}.

Results and discussion

Experimental setup. The antiferromagnetic layer of FeMn exchange biases the top layer of Py ($Ni_{80}Fe_{20}$), ensuring a stable AP-state (Fig. 1a). The Cu between the Nb and Py improves interface quality by limiting magnetic dead layers[39–41], and also increases the magnitude of magnetoresistance[38]. As Cu contact layers are used,

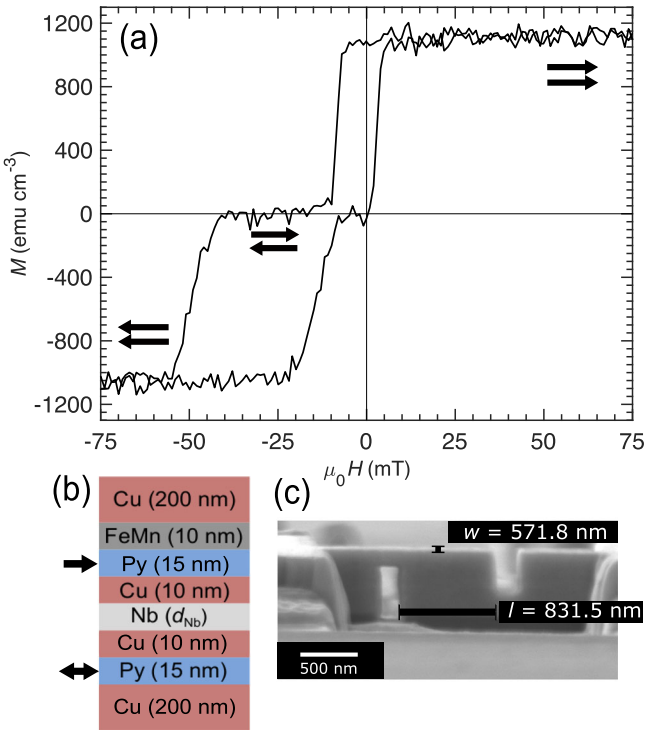

Fig. 1 Magnetic switching characteristics and device heterostructure. **a** Magnetization (M) vs. in-plane magnetic field (H) hysteresis loop for an unpatterned spin-valve at 10 K (arrows indicate the net magnetic moment directions of the top and bottom permalloy layers, μ_0 is the magnetic permeability in a vacuum). **b** Schematic diagram of the superconducting spin-valve with layer thicknesses, including varying Nb thickness d_{Nb}. Arrows represent pinned (top) and free (bottom) ferromagnetic layers. **c** Scanning electron micrograph of an example nanopillar spin-valve. `Length' ($l = 831.5 \pm 40$ nm) and `width' ($w = 571.8 \pm 40$ nm) of this device are labelled. Device area, $A = l \times w = 4.7 \pm 0.4 \times 10^5$ nm^2.

the section under measurement is not exclusively the nanopillar device, but includes part of the patterned structure from which the nanopillar was milled, which is 4 μm wide and 20 μm long (illustration available in Supplementary Methods). This section of heterostructure, referred to as the 'contact leads', contributes to the measured resistance and so we refer to the measurement as 'quasi' four-point. One important impact of this contact lead resistance is that $R(T)$ measurements can appear to contain two distinct superconducting transitions (Fig. 2a, d). The higher temperature transition ('contact transition') corresponds to the Nb in the contact leads, whereas the lower temperature transition ('device transition') corresponds to the nanopillar device. We define the onset temperature of the latter as T_{device}, and T_c as the temperature at 50% of the resistance change below T_{device} (Supplementary Note 4). Finally, in CPP measurements, since the cross-sectional areas (A) of the CPP spin-valves vary, ΔR is normalized by multiplying by A (i.e. $A\Delta R$)[5].

Device behaviour. $R(T)$ and $R(H)$ measurements of two devices are shown in Fig. 2. Whilst the normal state $R(H)$ loops (Fig. 2b, e) indicate GMR behaviour as expected, the superconducting state loops (Fig. 2c, f) reveal that two distinct behaviours appear in our devices, which is supported by the device transitions in Fig. 2a, d; for the device with higher $d_{Nb} = 28.5$ nm, $T_c(AP) < T_c(P)$ and $\Delta R > 0$, consistent with the results of Gu et al.[38], suggesting GMR moderated by quasiparticles (QP GMR). For the device with lower $d_{Nb} = 25$ nm ΔR is negative (Fig. 2c), and $T_c(P) < T_c(AP)$. These results are those expected for superconducting spin-valve effect behaviour observed in CIP

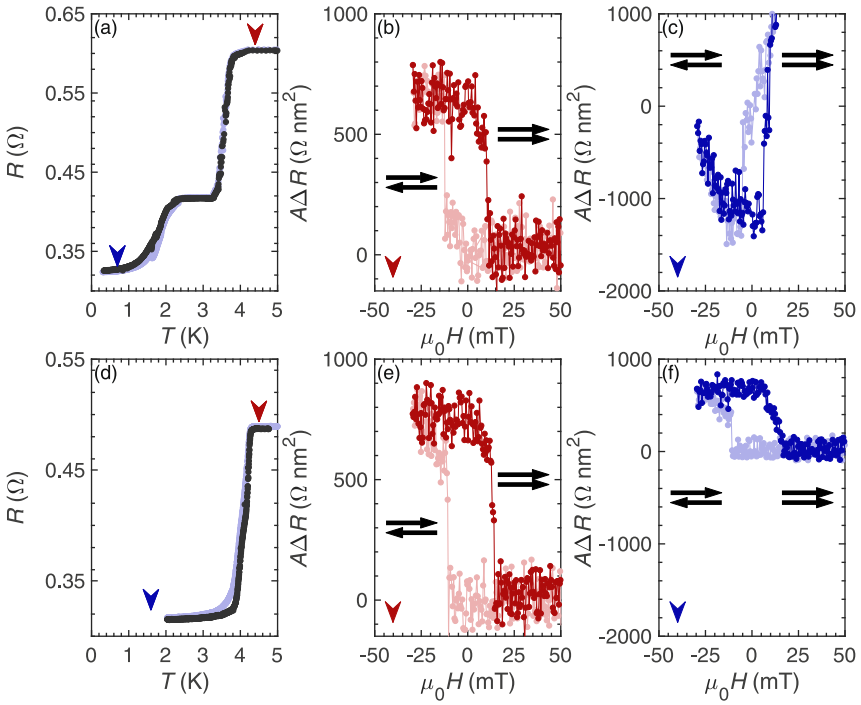

Fig. 2 R(T) and R(H) measurements for two spin-valve devices demonstrating different behaviours. The two different device responses observed. **a** Resistance (R) vs. temperature (T) curve for a device with Nb thickness $d_{Nb} = 25$ nm, in both the parallel (black) and antiparallel (blue) states. **b**, **c** Minor $R(H)$ loops (μ_0: magnetic permeability in a vacuum, H: in-plane magnetic field) from the same device as (**a**), in the normal state, (**b**), showing giant magnetoresistance, and the superconducting (**c**) state, which has greater resistance in the parallel state. **d** $R(T)$ curve for a device with $d_{Nb} = 28.5$ nm, in both the parallel (black) and antiparallel (blue) states. **e**, **f** Minor $R(H)$ loops from the same device as (**d**), in the normal state, (**e**), showing giant magnetoresistance, and the superconducting (**f**) state. In the superconducting state, the antiparallel state has higher resistance, similar to the normal state. For the $R(H)$ loops, light data represent sweeps from positive to negative H, starting at high positive values. The dark data in each loop is for the return sweep. In these minor loops, only the free permalloy layer undergoes switching, illustrated by the black arrows, which show the relative magnetic moment orientation of the permalloy layers. Arrows in **a**, **d** indicate the temperature of the corresponding $R(H)$ loops. Supplementary Fig. 1 features **b**, **f** with different axes, and Supplementary Fig. 2 features similar plots for two additional devices.

devices. The resistance increase with increasing field visible in Fig. 2c occurs for all superconducting spin-valve effect devices, which all have low H_{c2} values (being mid-transition at measurement temperatures), and therefore exhibit visible resistance increases within an applied magnetic field.

Normal state spin decay. In Fig. 3 we show the absolute value $A|\Delta R|$ versus d_{Nb}, with data points and y-error representing the mean of multiple devices from a single substrate and their standard deviation respectively. Grey data are from devices in their normal state (measured at < 10 K) and coloured data are from devices in the superconducting state at $T/T_{device} = 0.3$. Blue points are devices demonstrating the superconducting spin valve effect. By fitting a simple decaying exponential, $\exp(-d_{Nb}/l_{sf})$[42], a reasonable approximation where the thickness of the ferromagnet (15 nm) is much greater than the spin-flip length in the ferromagnet (5.5 nm[43]), we estimate spin-diffusion lengths from the GMR data in both the normal and superconducting states: $l_{sf}^{N} = 25 \pm 3$ nm, and $l_{sf}^{S} = 12 \pm 4$ nm. The decay length for QP GMR (in the superconducting state) is shorter than the normal state decay length, as found previously[38]. Normalised values of $\Delta R_{norm} = [R^{AP}(H = 0) - R^{P}(0)]/R^{P}(0)$ range from $\Delta R_{norm} = 0.00024$–$0.0045$ in the normal state, from $\Delta R_{norm} = 0.00032$–$0.0054$ for QP GMR devices, and from $\Delta R_{norm} = -0.011$ to -0.053 for devices demonstrating the superconducting spin valve effect.

Crossover. We now detail the main results of this article. To the best of our knowledge, the superconducting spin-valve effect has not been previously observed in CPP superconducting spin valves, and so we investigate the factors that determine the appearance of this effect.

In Fig. 4 we plot $A\Delta R$ at $T/T_{device} = 0.3$ versus d_{Nb}, which shows a systematic dependence of $A\Delta R$ on d_{Nb}, with a crossover from positive to negative $A\Delta R$ occurring at $d_{Nb} = 26$ nm. The inset shows the equivalent trend of ΔT_cversus d_{Nb}. For $d_{Nb} = 21$ nm, the superconducting spin valve effect reaches a positive ΔT_c up to 299 mK (Supplementary Note 1: Supplementary Fig. 2a), which is large for transition metal F/S/F spin-valves where values are usually of the order tens of mK[9–18,22–30]. However, we note that these large values of ΔT_c are linked to inflation of $A\Delta R$ (Supplementary Note 2); devices showing the superconducting spin-valve effect have suppressed and broadened device transitions (transition width > 1 K in Fig. 2a), meaning even these large ΔT_c values will not allow infinite magnetoresistance (complete switching between superconducting or normal states at a constant temperature). By considering the impact of superconductivity rather than just d_{Nb}, using T_{device} as the independent parameter, the outlier points at $d_{Nb} = 31$ nm were shown to agree far better with the overall trend in the data (Supplementary Note 1: Supplementary Fig. 4a and Supplementary Fig. 5). This led to consideration of the value $d_{Nb}/\xi_{S,d}$, where $\xi_{S,d}$ is the dirty limit coherence length in the superconductor, calculated using

$$\xi_{S,d} = \sqrt{\frac{\hbar D}{1.764 k_B T_{device}}},$$

where $D = 1.4 \times 10^{-4}$ m^{2}s^{-1} is the electron diffusivity, calculated from a coherence length measurement of an isolated 30 nm Nb film,

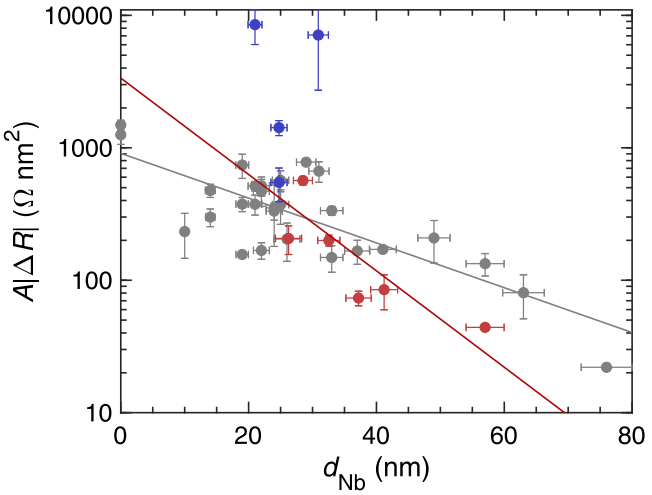

Fig. 3 Spin decay in the normal and superconducting states. $A|\Delta R|$ (device area A, magnetoresistance ΔR) vs. Nb thickness (d_{Nb}) in current perpendicular-to-plane spin valves for both the normal state (below 10 K, grey) and superconducting state ($T/T_{device} = 0.3$, red/blue, where T is temperature and T_{device} is the onset temperature of the device transition). Red circles are devices showing quasiparticle giant magnetoresistance, whereas blue circles show the superconducting spin valve effect. For clarity, points are the mean value from multiple devices on a single substrate; vertical error bars are the standard deviation in $A\Delta R$ of these devices and horizontal error bars the uncertainty in d_{Nb}. Supplementary Fig. 3 features this plot with devices plotted as individual points. Fits are a simple exponential decay considering each device individually, as described in the Normal state spin decay section.

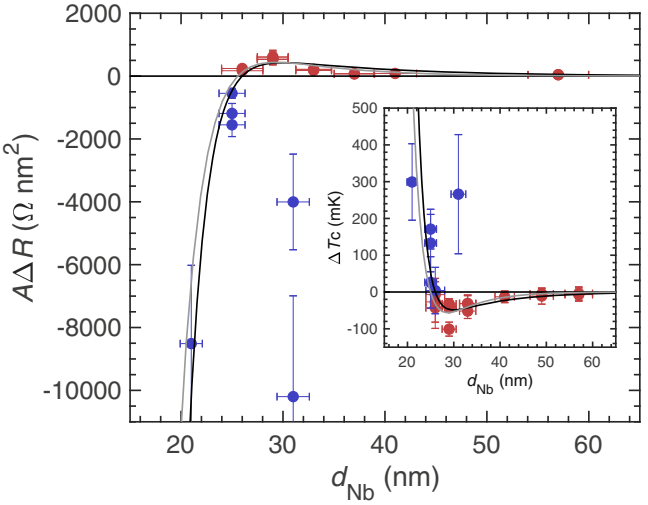

Fig. 4 Thickness (d_{Nb}) dependent crossover of superconducting state behaviour. $A\Delta R$ (device area A, magnetoresistance ΔR) at $T/T_{device} = 0.3$ vs. Nb thickness d_{Nb}, where T is temperature and T_{device} is the onset temperature of the device transition. The inset is the difference between superconducting critical temperatures in the parallel and antiparallel states, ΔT_c, vs. d_{Nb}. Red points show quasiparticle giant magnetoresistance dominated behaviour, blue the superconducting spin valve effect dominated behavior. Points represent individual spin-valve devices. Vertical error bars are the measurement uncertainty in $A\Delta R$ for each device and horizontal error bars the uncertainty in d_{Nb}. Curves are fits as described in the Phenomenological model section; grey curves fit with all parameters free, black with more limited parameters. The crossover point is $d_{Nb} = 26$ nm.

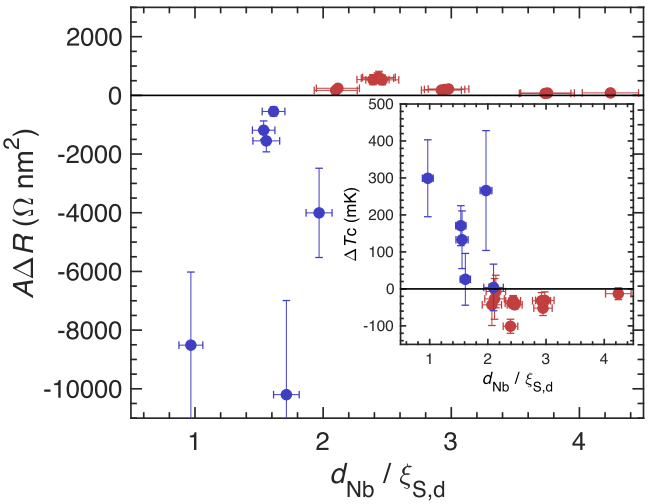

Fig. 5 Normalised thickness dependent crossover of superconducting state behaviour. $A\Delta R$ (device area A, magnetoresistance ΔR) at $T/T_{device} = 0.3$ vs. $d_{Nb}/\xi_{S,d}$, where T is temperature and T_{device} is the onset temperature of the device transition, d_{Nb} is Nb thickness and $\xi_{S,d}$ is dirty limit coherence length. The inset is the difference between superconducting critical temperatures in the parallel and antiparallel states, ΔT_c, vs. $d_{Nb}/\xi_{S,d}$. Red points show quasiparticle giant magnetoresistance dominated behaviour, blue the superconducting spin valve effect dominated behavior. Points represent individual spin-valve devices. Vertical error bars are the measurement uncertainty in $A\Delta R$ for each device and horizontal error bars the uncertainty in d_{Nb}. The crossover point between the two behaviours occurs around $d_{Nb} = 2\xi_{S,d}$.

and k_B is Boltzmann's constant. Using this normalised d_{Nb}, we account for both thickness and processing effects which may affect the superconductivity in the devices. Figure 5 shows $A\Delta R$ at $T/T_{device} = 0.3$ and (Inset) ΔT_c vs. $d_{Nb}/\xi_{S,d}$, which shows that the crossover between the two behaviours occurs at around $d_{Nb} = 2\xi_{S,d}$.

Both Figs. 4 and 5 show the same overall trend: with decreasing d_{Nb}, QP GMR (red) increases as expected, but then peaks and decreases rapidly, devices crossing over into superconducting spin-valve effect dominated behaviour, which rapidly increases in magnitude with decreasing d_{Nb}. The peak then fall shape of the trend indicates that rather than being a sudden switch from QP GMR to superconducting spin-valve effect behaviour, these are two separate effects which compete within the devices.

The crossover between positive and negative values of $A\Delta R$ is clear and the magnitude is significant, ruling out minor background effects. Scatter of the data does not account for the crossover behaviour, as indicated by a plot of ΔR at $T/T_{device} = 0.3$ normalised by ΔR in the normal state (Supplementary Note 1: Supplementary Fig. 4b).

Background effects. The 'double' transition visible within these devices highlights the contribution of the 'contact leads' to the measured resistance in these devices. It also highlights that the lower transition - the device transition - tends to be more suppressed in devices demonstrating the superconducting spin-valve effect compared to those demonstrating QP GMR (compare Fig. 2a, d, which feature device transitions around 2 K apart, whereas the 'contact' transitions differ by less than 1 K). This observation suggests not only d_{Nb}, but also the strength of superconducting order within the devices affect the appearance of the superconducting spin-valve effect.

Below their superconducting transition, the contact leads are superconducting and do not contribute to the measured $R(H)$ response, as shown in the inset to Fig. 6a, which was measured on the contact leads only. The exception to this is the substrate with thinnest $d_{Nb} = 21$ nm: even at the lowest temperatures, the contact leads demonstrate an $R(H)$ response which also shows the superconducting spin valve effect (Fig. 6a), which may contribute to the large magnitude of the measured effect for that device.

We have considered alternative explanations for the negative ΔR in our devices (Fig. 2e) including anisotropic magnetoresistance[44]. However, this is ruled out since anisotropic magnetoresistance is not observed in these superconducting spin-valve effect devices above T_c (Fig. 2b). Additionally, the zero field $R(T)$ measurements show distinct differences between P- and AP-states and anisotropic magnetoresistance would not lead to such differences in the absence of an applied magnetic field[3]. Negative magnetoresistance could also result from crossed Andreev reflection[45–49] of electrons across the superconducting layer, when the layer is less than one superconducting coherence length thick. Crossed Andreev reflection has previously been considered as a source of magnetoresistance in CIP spin valves[50], but is generally considered as a non-local effect. We note that there is one report of crossed Andreev reflection measured in a local setup[51], but the origin of magnetoresistance in this case is uncertain.

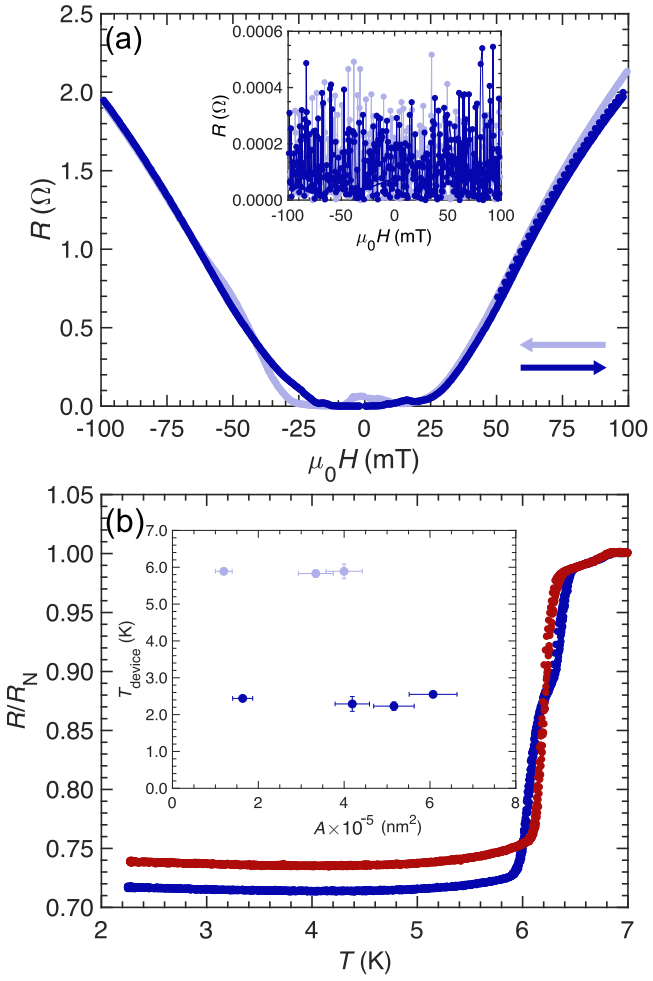

Fig. 6 Contact lead magnetoresistance and transition variation. a Major resistance (R) vs. in-plane magnetic field (H) loop measured on the contact leads at 0.3 K for the device with Nb thickness $d_{Nb} = 21$ nm (μ_0 is the magnetic permeability in a vacuum). For this device only, there is a negative (parallel state is higher resistance) magnetoresistance response in the contact leads at the measurement temperature. Inset: for all other devices, the leads are superconducting below the contact lead transition, and show no magnetoresistance response at $T/T_{device} = 0.3$, where T is temperature and T_{device} is the onset temperature of the device transition. **b** $R(T)$ curves from two devices on the same substrate $d_{Nb} = 57$ nm, normalised by their normal state resistance for comparison. The difference between the temperature of contact and device transitions varies in an unknown manner, and can be small enough that the two transitions are indistinguishable. Inset: T_{device} vs. nanopillar area, for a device showing the superconducting spin valve effect ($d_{Nb} = 25$ nm, dark blue) and a device showing quasiparticle giant magnetoresistance ($d_{Nb} = 37$ nm, light blue). Error bars represent measurement uncertainty.

The values for spin decay length calculated in our devices ($l_{sf}^{N} = 25 \pm 3$ nm, and $l_{sf}^{S} = 12 \pm 4$ nm) can be compared with other values from the literature. A similar CPP structure has been used previously[38] to measure values of $l_{sf}^{N} = 48 \pm 3$ nm and $l_{sf}^{S} = 17.5 \pm 0.6$ nm. Additionally, a value of $l_{sf}^{N} = 40 \pm 5$ nm was extracted from a fit to ferromagnetic resonance data[52]. These literature values are larger than the values measured here; we attribute this difference to increased scattering due to impurities and defects introduced during the nanopatterning process. These defects may also contribute to the separation of device and 'contact lead' superconducting transitions. This separation is inconsistent even between devices on the same substrate, as demonstrated in Fig. 6b, which we cannot currently explain. If the focused ion-beam milling were accountable for this transition separation, the separation would scale with nanopillar area. However, as shown in the inset to Fig. 6b, the transition temperature of the device transition, represented by the starting temperature T_{device}, does not demonstrate any dependence on device area. This uncertainty around the two transitions does not affect the main observation of this paper; the appearance of the superconducting spin valve effect in both $R(H)$ and $R(T)$ measurements and a thickness dependent crossover between them.

The comparison of positive magnetoresistance data above and below T_c supports the suggestion that CPP devices demonstrate QP GMR, as originally demonstrated by Gu et al.[38]. Similarly to that paper, we also observe a decrease in spin decay length in the superconducting state which is consistent with the additional impact of Andreev reflection causing decay of quasiparticles that cause this magnetoresistance. Unlike Gu et al.[38], we have also measured superconducting devices with d_{Nb} smaller than the thickness at which Andreev reflection does not appear to play a role. These devices are those that demonstrate the superconducting spin-valve effect, having negative $A\Delta R$. The crossover between these two effects appears to occur at around $d_{Nb} = 2\xi_{S,d}$, from Fig. 5, supported by the crossover thickness of $d_{Nb} = 26$ nm, which is close to twice $l_{sf}^{S} = 12 \pm 4$ nm, similar to the results of Gu et al.[38].

Phenomenological model. A simple model for this setup[38] assumes QP GMR in CPP F/S/F spin-valves decays due to Andreev reflection as quasiparticles pass a potential barrier with a temperature-dependent height i.e. $\Delta^{AP} = \Delta^{P} = \Delta(T)$, and reduced thickness $d_{Nb} - d_0$, where $d_0/2$ is the thickness of the region near each F/S interface where the superconducting gap and Andreev reflection are suppressed, expected to be equal to the coherence length. This approximation captures the QP GMR results in Fig. 4 beyond $d_{Nb} = 26$ nm, but cannot describe our superconducting spin-valve effect data.

We extend these ideas in a toy model that simply illustrates the two competing effects within our devices, capturing the overall trend as the difference of two exponential decays,

$$\Delta R = A \exp\left[\frac{-(d_{Nb} - d_0)}{l_S}\right] - B \exp\left[\frac{-(d_{Nb} - d_0)}{\Lambda_S}\right]$$

where the first term relates to QP GMR ($\Delta R > 0$), as in the model from[38] and the second to the superconducting spin valve effect ($\Delta R < 0$), with a characteristic decay Λ_S. In the thinner Nb regime of our data, $T_c(AP) > T_c(P)$ meaning that the superconducting spin-valve effect enhances Δ^{AP}[7,8]; leading to decreased resistance as a greater proportion of the Nb is superconducting. We choose an exponential for this decay to reproduce the distinct shape of the data in Fig. 4, but note that a different thickness dependence may also be usable to describe the data, and the superconducting spin valve effect in particular. Here, our aim is to demonstrate that two competing effects can describe this crossover, rather than to definitively model the trend, as theoretical development of the interaction of these effects will be necessary for such a model. Initially, we fit this model with all parameters free and find values as an average and deviation from orthogonal distance regression on the $A\Delta R$ and ΔT_c data, which fits both data sets. We find $d_0 = 28.8 \pm 4.4$ nm, $l_S = 7.1 \pm 2.0$ nm and $\Lambda_S = 2.2 \pm 1.2$ nm, with the resulting curves shown in grey in Fig. 4. Whilst this curve successfully illustrates that two competing effects can be responsible for this dependence on d_{Nb}, we were also interested to see if the same could be achieved by linking the parameters to more physical values (further information on our model fitting is reported in Supplementary Note 3). We set $d_0 = 26$ nm, the crossover thickness, causing $|A/B| = 1$, and set l_S to the value $l_{sf}^S = 12$ nm. We find a value for $\Lambda_S = 2.2 \pm 0.7$ nm, resulting in the black curve in the main plot and inset of Fig. 4, and demonstrating that physical values used in the model can still give rise to the key peak in the data. The $\Lambda_S = 2.2 \pm 0.7$ nm value is very small and does not initially appear to represent a physical length, unlike l_S and d_0; however, we note previous superconducting spin-valve investigations[11] have seen a dramatic shift from a ΔT_c of 41 mK to "only a few mK" for an increase in d_{Nb} of only 1 nm, which could only be modelled by theory using parameters that did not match the estimates of the authors. These short decay lengths may reflect some experimental effects not accounted for by theory based fits, but due to the uncertainty within the model, such as alternative dependencies that could be used, we do not feel these values and the model should be considered more than illustration of the potential for a more complete theory of this system.

The toy model illustrates coexistence of the superconducting spin-valve effect and QP GMR, which compete within these devices. We believe that whilst the two effects of superconducting spin-valve effect and QP GMR are not strictly linked, both heavily depend on the coherence length. The crossover thickness d_0 occurs at roughly twice the coherence length, as suggested in Fig. 5, and the QP GMR decay length l_S is dominated by the coherence length as found previously[38].

Previous studies showing both positive and negative values of ΔR are explained on the basis of stray magnetic fields or vortex flow from a multi-domain state of one or both coupled F layers[14,29,53]. In our spin-valves positive ΔR is expected due to QP GMR, and a multidomain state with out-of-plane stray magnetic fields would cause positive magnetoresistance within the transition region, which is far from the measurement temperature of our QP GMR data (Fig. 2b). No studies that we are aware of have demonstrated a systematic change of sign of magnetoresistance with d_{Nb}, such as the crossover we show here.

Conclusion

In summary, we have presented evidence for a competition between QP GMR and the superconducting spin valve effect in superconducting CPP spin-valves. Below a Nb thickness of $d_{Nb} \approx 26$ nm, ΔR is negative and determined by the superconducting spin valve effect; beyond this critical thickness, ΔR is positive with a magnitude that is determined by QP Andeev reflection. Figure 5 suggests this thickness appears to correspond to twice the dirty limit coherence length of the devices. These results are relevant to development of quasiparticle spintronics devices, suggesting devices utilising QP GMR effects should be fabricated with $d_{Nb} > 26$ nm, or consider using the superconducting spin valve effect.

Methods

Pillar fabrication. Heterostructures are deposited by dc magnetron sputtering in an ultra-high vacuum chamber with a base pressure better than 10^{-8} mbar. Films are deposited onto (001) single crystal silicon with a 250 nm-thick surface oxide, with an in-plane magnetic field (100 mT) applied during growth to set in-plane uniaxial anisotropy. Powers of 60 W are used for Cu contact layers and the bottom Py layer, 15 W for other Cu layers and 30 W for all other layers.

The spin-valves are patterned into nanopillars using optical lithography and Ar-ion milling to form a wire pattern, followed by Ga-ion focused ion-beam etching[54] to form the pillars. A 100 pA beam current is used to thin down a wire section, followed by a wall cleaning step with a 10 pA beam current. The beam angle is then changed so that it is parallel to the surface of the substrate to enable cuts into the heterostructure to isolate the nanopillar from the rest of the 'wire' section. To enable this rotation, the substrate is mounted on a custom 45° wedge holder. The lengths and widths of the nanopillars vary between 400–1500 nm and 300–1000 nm, respectively. Dimension and resistance values for each device are reported in Supplementary Table 1, and Supplementary Fig. 9 illustrates the focused ion-beam steps.

Measurement. Resistance of the CPP spin-valves vs. temperature [$R(T)$] or in-plane magnetic field [$R(H)$] is measured using a 'quasi' four-point current-bias setup in a pulse-tube measurement system, which removes contact resistance. Measurements were made on devices in both the normal state (above the superconducting transition of the nanopillar device and contact leads, but below 10 K) and in the superconducting state, although many devices had such a suppressed transition temperature that they could not be measured in the superconducting state. The current used was 50 μA, which is not large enough to affect the superconducting critical temperature.

Data availability

The raw measurement data that support the findings of this study and are used for all figures are available in Apollo, the University of Cambridge repository with the identifier https://doi.org/10.17863/CAM.84715.

Received: 21 January 2022; Accepted: 24 August 2022;
Published online: 10 September 2022

References

1. Žutić, I., Fabian, J. & Das Sarma, S. Spintronics: Fundamentals and applications. *Rev. Mod. Phys.* **76**, 323–410 (2004).
2. Johnson, M. & Silsbee, R. H. Interfacial charge-spin coupling: Injection and detection of spin magnetization in metals. *Phys. Rev. Lett.* **55**, 1790–1793 (1985).
3. Dieny, B. et al. Giant magnetoresistive in soft ferromagnetic multilayers. *Phys. Rev. B* **43**, 1297–1300 (1991).
4. Valet, T. & Fert, A. Classical theory of perpendicular giant magnetoresistance in magnetic multilayers. *J. Magn. Magn. Mater.* **121**, 378–382 (1993).
5. Bass, J. CPP magnetoresistance of magnetic multilayers: A critical review. *J. Magn. Magn. Mater.* **408**, 244–320 (2016).
6. Oh, S., Youm, D. & Beasley, M. R. A superconductive magnetoresistive memory element using controlled exchange interaction. *Appl. Phys. Lett.* **71**, 2376–2378 (1997).
7. Tagirov, L. R. Low-field superconducting spin switch based on a superconductor /ferromagnet multilayer. *Phys. Rev. Lett.* **83**, 2058–2061 (1999).
8. Buzdin, A. & Vedyayev, A. Spin-orientation-dependent superconductivity in F / S / F structures. *Europhys. Lett.* **48**, 686–691 (1999).
9. Gu, J. Y. et al. Magnetization-orientation dependence of the superconducting transition temperature in the ferromagnet-superconductor-ferromagnet system: CuNi/Nb/CuNi. *Phys. Rev. Lett.* **89**, 267001 (2002).
10. Potenza, A. & Marrows, C. H. Superconductor-ferromagnet CuNi/Nb/CuNi trilayers as superconducting spin-valve core structures. *Phys. Rev. B* **71**, 180503(R) (2005).

11. Moraru, I. C., Pratt, W. P. & Birge, N. O. Magnetization-Dependent Tc Shift in Ferromagnet/Superconductor/Ferromagnet Trilayers with a Strong Ferromagnet. *Phys. Rev. Lett.* **96**, 037004 (2006).
12. Moraru, I. C., Pratt, W. P. & Birge, N. O. Observation of standard spin-switch effects in ferromagnet/superconductor/ ferromagnet trilayers with a strong ferromagnet. *Phys. Rev. B* **74**, 220507(R) (2006).
13. Miao, G.-X., Ramos, A. V. & Moodera, J. S. Infinite Magnetoresistance from the Spin Dependent Proximity Effect in Symmetry Driven bcc-Fe/V/Fe Heteroepitaxial Superconducting Spin Valves. *Phys. Rev. Lett.* **101**, 137001 (2008).
14. Zhu, J., Cheng, X., Boone, C. & Krivorotov, I. N. Origin of the inverse spin switch effect in superconducting spin valves. *Phys. Rev. Lett.* **103**, 027004 (2009).
15. Leksin, P. V. et al. Full spin switch effect for the superconducting current in a superconductor/ferromagnet thin film heterostructure. *Appl. Phys. Lett.* **97**, 102505 (2010).
16. Zhu, J., Krivorotov, I. N., Halterman, K. & Valls, O. T. Angular dependence of the superconducting transition temperature in ferromagnet-superconductor-ferromagnet trilayers. *Phys. Rev. Lett.* **105**, 207002 (2010).
17. Leksin, P. V. et al. Superconducting spin-valve effect and triplet superconductivity in CoOx/Fe1/Cu/Fe2/Cu/Pb multilayer. *Phys. Rev. B* **91**, 214508 (2015).
18. Jara, A. A., Moen, E., Valls, O. T. & Krivorotov, I. N. Bias current dependence of superconducting transition temperature in superconducting spin-valve nanowires. *Phys. Rev. B* **100**, 184512 (2019).
19. Gu, Y., Halász, G. B., Robinson, J. W. A. & Blamire, M. G. Large superconducting spin valve effect and ultrasmall exchange splitting in epitaxial rare-earth-Niobium Trilayers. *Phys. Rev. Lett.* **115**, 067201 (2015).
20. Li, B. et al. Superconducting spin switch with infinite magnetoresistance induced by an internal exchange field. *Phys. Rev. Lett.* **110**, 097001 (2013).
21. Zhu, Y., Pal, A., Blamire, M. G. & Barber, Z. H. Superconducting exchange coupling between ferromagnets. *Nat. Mater.* **1**, 1–6 (2016).
22. Aarts, J. & Rusanov, A. Y. The effects of magnetization switching on the superconducting properties of S/F bilayers and F/S/F trilayers. *Comptes Rendus Phys.* **7**, 99–106 (2006).
23. Rusanov, A. Y., Habraken, S. & Aarts, J. Inverse spin switch effects in ferromagnet-superconductor-ferromagnet trilayers with strong ferromagnets. *Phys. Rev. B* **73**, 060505(R) (2006).
24. Steiner, R. & Ziemann, P. Magnetic switching of the superconducting transition temperature in layered ferromagnetic/superconducting hybrids: Spin switch versus stray field effects. *Phys. Rev. B* **74**, 094504 (2006).
25. Singh, A., Sürgers, C. & Löhneysen, H. V. Superconducting spin switch with perpendicular magnetic anisotropy. *Phys. Rev. B* **75**, 024513 (2007).
26. Singh, A. et al. Spin-polarized current versus stray field in a perpendicularly magnetized superconducting spin switch. *Appl. Phys. Lett.* **91**, 71–74 (2007).
27. Stamopoulos, D., Manios, E. & Pissas, M. Stray-fields-based magnetoresistance mechanism in $ni_{80}fe_{20} - Nb - ni_{80}fe_{20}$ trilayered hybrids. *Phys. Rev. B* **75**, 184504 (2007).
28. Leksin, P. V. et al. Observation of the "Inverse" spin valve effect in a Ni/V/Ni trilayer system. *JETP Lett.* **90**, 59–63 (2009).
29. Hwang, T. J., Kim, D. H. & Oh, S. Observation of a transition from inverse-spin-switch to spin-switch behavior in domain state of a Py/Nb/Py trilayer. *IEEE Trans. Magn.* **46**, 235–238 (2010).
30. Flokstra, M., van der Knaap, J. M. & Aarts, J. Magnetic coupling in superconducting spin valves with strong ferromagnets. *Phys. Rev. B* **82**, 184523 (2010).
31. Takahashi, S., Imamura, H. & Maekawa, S. Spin Imbalance and Magnetoresistance in Ferromagnet/Superconductor/Ferromagnet Double Tunnel Junctions. *Phys. Rev. Lett.* **82**, 3911–3914 (1999).
32. Takahashi, S. & Maekawa, S. Spin injection and detection in magnetic nanostructures. *Phys. Rev. B* **67**, 052409 (2003).
33. De Simoni, G., Strambini, E., Moodera, J. S., Bergeret, F. S. & Giazotto, F. Toward the Absolute Spin-Valve Effect in Superconducting Tunnel Junctions. *Nano Lett.* **18**, 6369–6374 (2018).
34. Pratt, W. P. et al. Perpendicular giant magnetoresistances of Ag/Co multilayers. *Phys. Rev. Lett.* **66**, 3060–3063 (1991).
35. Lee, S. F. et al. Current-perpendicular and current-parallel giant magnetoresistances in Co/Ag multilayers. *Phys. Rev. B* **52**, 15426–15441 (1995).
36. Gijs, M. A. et al. Perpendicular giant magnetoresistance of microstructured pillars in FeCr and CoCu magnetic multilayers. *Mater. Sci. Eng. B* **31**, 85–92 (1995).
37. Eid, K. et al. Absence of mean-free-path effects in the current-perpendicular-to-plane magnetoresistance of magnetic multilayers. *Phys. Rev. B* **65**, 054424 (2002).
38. Gu, J. Y., Caballero, J. A., Slater, R. D., Loloee, R. & Pratt, W. P. Direct measurement of quasiparticle evanescent waves in a dirty superconductor. *Phys. Rev. B* **66**, 140507(R) (2002).
39. Bell, C., Loloee, R., Burnell, G. & Blamire, M. G. Characteristics of strong ferromagnetic Josephson junctions with epitaxial barriers. *Phys. Rev. B* **71**, 180501(R) (2005).
40. Robinson, J. W. A., Piano, S., Burnell, G., Bell, C. & Blamire, M. G. Zero to π transition in superconductor-ferromagnet-superconductor junctions. *Phys. Rev. B* **76**, 094522 (2007).
41. Tateishi, G. & Bergmann, G. Nickel on lead, magnetically dead or alive? *Eur. Phys. J. B* **73**, 155–160 (2010).
42. Park, W. et al. Measurement of resistance and spin-memory loss (spin relaxation) at interfaces using sputtered current perpendicular-to-plane exchange-biased spin valves. *Phys. Rev. B* **62**, 1178–1185 (2000).
43. Vila, L. et al. Current perpendicular magnetoresistances of NiFeCo and NiFe "permalloys". *J. Appl. Phys.* **87**, 8610–8614 (2000).
44. Mcguire, T. R. & Potter, R. I. Anisotropic Magnetoresistance in Ferromagnetic 3D Alloys. *IEEE Trans. Magn.* **11**, 1018–1038 (1975).
45. Deutscher, G. & Feinberg, D. Coupling superconducting-ferromagnetic point contacts by Andreev reflections. *Appl. Phys. Lett.* **76**, 487–489 (2000).
46. Beckmann, D., Weber, E. B. & Löhneysen, H. V. Evidence for crossed andreev reflection in superconductor-ferromagnet hybrid structures. *Phys. Rev. Lett.* **93**, 197003 (2004).
47. Beckmann, D. & Löhneysen, H. V. Negative four-terminal resistance as a probe of crossed Andreev reflection. *Appl. Phys. A Mater. Sci. Process.* **89**, 603–607 (2007).
48. Kleine, A., Baumgartner, A., Trbovic, J. & Schönenberger, C. Contact resistance dependence of crossed Andreev reflection. *Europhys. Lett.* 87 (2009).
49. Webb, J. L., Hickey, B. J. & Burnell, G. Numerical model of crossed Andreev reflection and charge imbalance. *Phys. Rev. B* **86**, 054525 (2012).
50. Giazotto, F., Taddei, F., Beltram, F. & Fazio, R. Crossed andreev reflection-induced magnetoresistance. *Phys. Rev. Lett.* **97**, 087001 (2006).
51. Cadden-Zimansky, P., Jiang, Z. & Chandrasekhar, V.Charge imbalance, crossed Andreev reflection and elastic co-tunnelling in ferromagnet/superconductor/normal-metal structures. *New J. Phys.* 9 (2007).
52. Jeon, K.-R. et al. Enhanced spin pumping into superconductors provides evidence for superconducting pure spin currents. *Nat. Mater.* **17**, 499–503 (2018).
53. Hwang, T. J. & Kim, D. H. Influence of stray fields and the proximity effect in ferromagnet/superconductor/ferromagnet spin valves. *J. Korean Phys. Soc.* **61**, 1628–1632 (2012).
54. Bell, C. et al. Fabrication of nanoscale heterostructure devices with a focused ion beam microscope. *Nanotechnology* **14**, 630–632 (2003).

Acknowledgements

This work was funded by the EPSRC through a DTP Studentship (nos. EP/M508007/1 and EP/N509620/1) and Programme Grant (no. EP/N017242/1).

Author contributions

B.S-S. conceived and designed the experiments with J.W.A.R's supervision. B.S-S. fabricated all devices and carried out all measurements. B.S-S. and X.M. developed the model. B.S-S. and J.W.A.R. wrote the manuscript, on which X.M. and M.G.B. commented. All authors discussed the results.

Competing interests

The authors declare no competing interests.

Additional information

Supplementary information The online version contains supplementary material available at https://doi.org/10.1038/s42005-022-01003-0.

Correspondence and requests for materials should be addressed to B. Stoddart-Stones or J. W. A. Robinson.

Peer review information *Communications Physics* thanks Matthias Althammer and the other, anonymous, reviewer(s) for their contribution to the peer review of this work.